applied sciences

MDPI

Article

Scattering of Plane Waves by Cylindrical Cavity in Unsaturated Poroelastic Medium †

Weihua Li [1,*], Zhe Yang [2], Aichen Zhang [2] and Fengcui Feng [2]

[1] Key Laboratory of Urban Underground Engineering of Ministry of Education, Beijing Jiaotong University, Beijing 100044, China
[2] School of Civil Engineering, Beijing Jiaotong University, Beijing 100044, China
* Correspondence: whli@bjtu.edu.cn
† This paper is an extended version of paper published in the conference: Proceedings of the 4th International Conference on Performance Based Design in Earthquake Geotechnical Engineering, Beijing, China, 15–17 July 2022.

Abstract: The scattering of elastic waves by underground cavities is an active research topic for its broad applications in various fields, such as earthquake engineering, the blast resistance of underground structures, geophysical exploration, etc. In most previous studies, the sounding medium was treated as an ideal elastic medium or a saturated poroelastic medium. The understanding of the scattering of elastic waves by cavities in unsaturated porous media is limited. In this study, the scattering of plane P_1 waves and SV waves by a cavity with a permeable surface in an infinite unsaturated porous medium is solved by the wave function expansion method. The dynamic stress concentration at the cavity surface is investigated by taking P_1 wave incidence, for example. Numerical results illustrate that the scattering of plane waves around the cavity strongly depends on the frequency of the incident waves, and the saturation, Poisson's ratio, and porosity of the surrounding medium.

Keywords: unsaturated porous media; cylindrical cavity; plane waves; scattering and diffraction; analytic solutions

check for updates

Citation: Li, W.; Yang, Z.; Zhang, A.; Feng, F. Scattering of Plane Waves by Cylindrical Cavity in Unsaturated Poroelastic Medium. *Appl. Sci.* **2023**, *13*, 494. https://doi.org/10.3390/app13010494

Academic Editors: Jian-Min Zhang, Arcady Dyskin, Lanmin Wang and Rui Wang

Received: 26 August 2022
Revised: 16 November 2022
Accepted: 2 December 2022
Published: 30 December 2022

Copyright: © 2022 by the authors. Licensee MDPI, Basel, Switzerland. This article is an open access article distributed under the terms and conditions of the Creative Commons Attribution (CC BY) license (https://creativecommons.org/licenses/by/4.0/).

1. Introduction

Nowadays, many underground structures such as subways, water-conveyance tunnels, mineral prospecting, and military facilities have been constructed all around the world. In earthquake events, seismic action may cause great damage to underground structures. The existence of underground cavities will cause wave scattering and stress concentration around the cavities, so as to change the seismic response of underground structures. Therefore, theoretical studies on the scattering of seismic waves by a cavity or tunnel are not only meaningful in revealing the induced amplification of and reduction in earthquake motion but are also helpful in guiding its anti-seismic design in a qualitative way.

In previous studies, scholars have carried out detailed research on the dynamic response characteristics of the soil around underground cavities. Initially, when considering the fluctuation of an elastic medium, the soil is usually simplified as a pure elastic medium without considering the influence of pores in the soil. For example, Pao and Mow [1] studied the dynamic response of a lined tunnel embedded in an infinite elastic medium, subjected to an incident wave; Lee with his cooperators [2–4] carried out a series of works to investigate the scattering of the P-wave, SH-wave, and SV-wave by a cavity or a circular tunnel in a half-space. For some water-rich grounds, underground structures are usually contained in a porous medium, which is filled with fluids in the pores. The presence of the fluids will significantly affect the mechanical behavior of the tunnels. To illustrate the influence of the fluids, on the basis of Biot's model [5], Mei et al. [6] investigated the wave scattering by a circular cavity in a saturated porous medium by using the boundary layer approximation. Krutin et al. [7] studied the wave propagation of a plane harmonic wave

disturbed by a fluid-filled cylindrical cavity in a saturated porous medium. Shiba and Okamoto [8] proposed a method to analyze the dynamic response of cylindrical tunnels within the soft ground. The mechanical responses of lined and non-lined tunnels under a harmonic wave were investigated by Kattis et al. [9]. Li and Zhao [10] solved the problem of plane wave scattering from cylindrical cavities in the saturated poroelastic half-space using the wave function expansion method. Jiang et al. [11] solve the two-dimensional scattering of plane waves by a lined cylindrical cavity in the poroelastic half-plane approximating the half-plane surface as a convex circular surface. Xu et al. [12] investigated the wave scattering by a shallowly buried lining in a poroelastic half-space considering the non-local effect. As can be seen in Ref. [13], the research on the scattering of seismic waves by underground caverns in saturated media is well understood.

However, in reality, unsaturated poroelastic media are encountered in many areas. In general cases, two types of fluids coexist within the porous space: either two liquids, such as oil and water in oil fields, or a gas and a liquid, such as air and water in unsaturated soil geomaterials. Therefore, studying the dynamic responses in unsaturated porous media is of considerable interest. As summarized by Li et al. [14], numerous unsaturated poroelasticity models have been established, and the dynamic behaviors of unsaturated porous media have been studied. According to these studies, the dynamic response of an unsaturated medium is significantly different from that of a traditional saturated porous medium in many respects owing to the existence of the gas phase. However, to date, there have several reports on the dynamic responses of underground cavities in unsaturated poroelastic media. Li et al. [15] considered the transient responses of pressurized cylindrical unlined and lined cavities in an infinite unsaturated poroelastic medium for the first time. According to the analysis, saturation has a significant influence on the responses of the radial displacements, hoop stresses, and pore fluid pressures at the cavity surface. In considering the scattering problem of plane P wave disturbed by a lined tunnel embedded in an infinite unsaturated poroelastic medium, Tan et al. [16] also showed that the degree of saturation plays an important role in the dynamic response of the lined tunnel in the unsaturated porous medium. All of these reminded us that the effects of saturation on dynamic responses of underground cavities in unsaturated porous media may need to be carefully considered.

The authors presented the analytical solution of the scattering of plane waves by a cylindrical cavity with an impermeable surface and analyzed the effects of saturation on the dynamic responses around the cavity in the paper submitted to the Special Issue of PBD-IV [17]. In this study, the scattering of plane P_1 waves and SV waves by a cylindrical cavity with a permeable surface in an infinite unsaturated porous medium is solved based on Ref. [17]. The dynamic stress concentration of the cavity surface is investigated according to the solutions. A detailed parametric study is presented to illustrate the influence of the degree of saturation, porosity, and Poisson's ratio on the dynamic stress concentration of the hoop stresses at the cavity surface under different conditions.

2. Model and Solution

2.1. Mathematical Models and Basic Equations

A long cylindrical cavity of radius $r = a$ in an infinite unsaturated porous medium is considered as shown in Figure 1. The hydraulic boundary conditions at the cavity surface are permeable. The dynamic equations for unsaturated porous media established by Wei and Muraleetharan [18] are applied to the model, which is expressed as:

$$\begin{aligned} n_0^S\rho_0^S\ddot{\boldsymbol{u}}^S &= \left(M_{SS}+n_0^S\mu_S\right)\nabla\nabla\cdot\boldsymbol{u}^S+n_0^S\mu_S\nabla\cdot\nabla\boldsymbol{u}^S+M_{SW}\nabla\nabla\cdot\boldsymbol{u}^W+M_{SN}\nabla\nabla\cdot\boldsymbol{u}^N \\ &\quad +\hat{\mu}^W\left(\dot{\boldsymbol{u}}^W-\dot{\boldsymbol{u}}^S\right)+\hat{\mu}^N\left(\dot{\boldsymbol{u}}^N-\dot{\boldsymbol{u}}^S\right) \\ n_0^W\rho_0^W\ddot{\boldsymbol{u}}^W &= M_{SW}\nabla\nabla\cdot\boldsymbol{u}^S+M_{WW}\nabla\nabla\cdot\boldsymbol{u}^W+M_{WN}\nabla\nabla\cdot\boldsymbol{u}^N-\hat{\mu}^W\left(\dot{\boldsymbol{u}}^W-\dot{\boldsymbol{u}}^S\right) \\ n_0^N\rho_0^N\ddot{\boldsymbol{u}}^N &= M_{SN}\nabla\nabla\cdot\boldsymbol{u}^S+M_{WN}\nabla\nabla\cdot\boldsymbol{u}^W+M_{NN}\nabla\nabla\cdot\boldsymbol{u}^N-\hat{\mu}^N\left(\dot{\boldsymbol{u}}^N-\dot{\boldsymbol{u}}^S\right) \end{aligned} \tag{1}$$

where the superscript S is the solid component; W and N are the wetting and non-wetting fluids, respectively; μ_S is the shear modulus of the unsaturated porous medium; and n_0^α,

ρ_0^α and $\boldsymbol{u}^\alpha(\alpha = \mathrm{S,W,N})$ are the initial volume fraction, initial density, and displacements of individual components, respectively. M_{SS}, M_{WW}, M_{NN}, M_{SW}, M_{SN} and M_{WN} are elastic coefficients related to the bulk modulus $K^\alpha(\alpha = \mathrm{S,W,N})$ of the various phases in unsaturated porous media, the bulk modulus of the solid skeleton $\hat{K}$, the shear modulus of the solid skeleton G, the effective stress coefficient α_B, and Poisson's ration v. $\hat{\mu}^f(f = W, N)$ is the soil water characteristic curve, which can be related to the intrinsic permeability of the porous medium k and the dynamic viscosity v^f of the f-fluid by the expressions given explicitly in Wei and Muraleetharan [18].

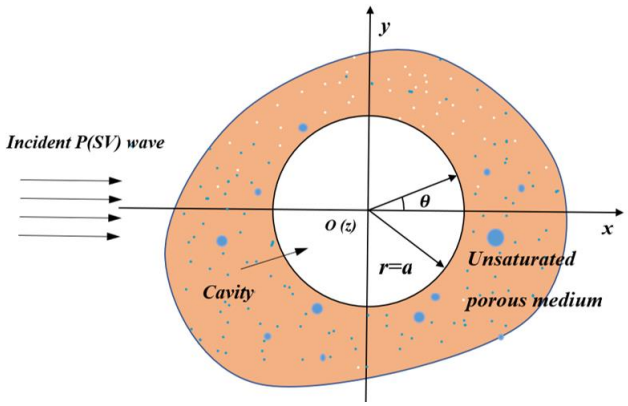


Figure 1. Cylindrical cavity in unsaturated medium.

The V g model to express the soil-water characteristic curve proposed by van Genuchten [19] is applied here:

$$p^{\mathrm{N}} - p^{\mathrm{W}} = \alpha^{-1}\left(S_{\mathrm{e}}{}^{-1/m} - 1\right)^{1-m} \tag{2}$$

where α and m are the van Genuchten model parameters depending on the properties of the three-phase model, and the effective degree of saturation, S_{e}, given by:

$$S_{\mathrm{e}} = \begin{cases} 0 & S_{\mathrm{r}} \le S_{\mathrm{rN}} \\ \frac{S_{\mathrm{r}} - S_{\mathrm{rW}}}{S_{\mathrm{rN}} - S_{\mathrm{rW}}} & S_{\mathrm{rW}} \le S_{\mathrm{r}} \le S_{\mathrm{rN}} \\ 1 & S_{\mathrm{r}} \ge S_{\mathrm{rN}} \end{cases} \tag{3}$$

where S_{r} represents the saturation of the unsaturated porous medium, S_{rW} represents the irreducible degree of saturation, and S_{rN} represents the air-entry degree of saturation.

Based on the poroelastic model proposed by Wei and Muraleetharan [18], the stress tensor in an unsaturated porous medium is expressed by:

$$\left.\begin{aligned} \boldsymbol{\sigma}^S &= \left(M_{SS}\nabla\cdot\boldsymbol{u}^S + M_{SW}\nabla\cdot\boldsymbol{u}^{\mathrm{W}} + M_{\mathrm{SN}}\nabla\cdot\boldsymbol{u}^{\mathrm{N}}\right)I + 2n_0^{\mathrm{S}}\mu_{\mathrm{S}}\left[\nabla\boldsymbol{u}^{\mathrm{S}} + \left(\nabla\boldsymbol{u}^{\mathrm{S}}\right)^T\right] \\ \boldsymbol{\sigma}^W &= \left(M_{SW}\nabla\cdot\boldsymbol{u}^S + M_{WW}\nabla\cdot\boldsymbol{u}^{\mathrm{W}} + M_{\mathrm{WN}}\nabla\cdot\boldsymbol{u}^{\mathrm{N}}\right)\boldsymbol{I} \\ \boldsymbol{\sigma}^N &= \left(M_{SN}\nabla\cdot\boldsymbol{u}^S + M_{WN}\nabla\cdot\boldsymbol{u}^{\mathrm{W}} + M_{\mathrm{NN}}\nabla\cdot\boldsymbol{u}^{\mathrm{N}}\right)\boldsymbol{I} \end{aligned}\right\} \tag{4}$$

In which $\boldsymbol{\sigma}^\alpha((\alpha = S, W, N)$ represents the stress tensors of each phase, and $\boldsymbol{I}$ denote the unit tensor matrix.

2.2. Solution of Dynamic Equation of Unsaturated Porous Media

Based on the Helmholtz theorem, the displacement vector $\boldsymbol{u}$ may be expressed as:

$$\boldsymbol{u}^\alpha = \nabla\varphi^\alpha + \nabla\times\boldsymbol{\Psi}^\alpha(\alpha = S, W, N) \tag{5}$$

where, φ^α, $\boldsymbol{\Psi}^\alpha(\alpha = S, W, N)$ are scalar potentials and vector potentials of α phase in unsaturated porous media, respectively.

By introducing Equation (5), Equation (1) is transformed into:

$$\begin{cases} n_0^S\rho_0^S\frac{\partial^2\varphi^S}{\partial t^2} = \left(M_{SS}+2n_0^S\mu_S\right)\nabla^2\varphi^S + M_{SW}\nabla^2\varphi^W + M_{SN}\nabla^2\varphi^N \\ \qquad\qquad +\hat{\mu}^W\left(\frac{\partial\varphi^W}{\partial t}-\frac{\partial\varphi^S}{\partial t}\right)+\hat{\mu}^N\left(\frac{\partial\varphi^N}{\partial t}-\frac{\partial\varphi^S}{\partial t}\right) \\ n_0^W\rho_0^W\frac{\partial^2\varphi^W}{\partial t^2} = M_{SW}\nabla^2\varphi^S + M_{WW}\nabla^2\varphi^W + M_{WN}\nabla^2\varphi^N - \hat{\mu}^W\left(\frac{\partial\varphi^W}{\partial t}-\frac{\partial\varphi^S}{\partial t}\right) \\ n_0^N\rho_0^N\frac{\partial^2\varphi^N}{\partial t^2} = M_{SN}\nabla^2\varphi^S + M_{WN}\nabla^2\varphi^W + M_{NN}\nabla^2\varphi^N - \hat{\mu}^N\left(\frac{\partial\varphi^N}{\partial t}-\frac{\partial\varphi^S}{\partial t}\right) \end{cases} \tag{6}$$

$$\begin{cases} n_0^S\rho_0^S\frac{\partial^2\boldsymbol{\Psi}^S}{\partial t^2} = n_0^S\mu_S\nabla^2\boldsymbol{\Psi}^S + \hat{\mu}^W\left(\frac{\partial\boldsymbol{\Psi}^W}{\partial t}-\frac{\partial\boldsymbol{\Psi}^S}{\partial t}\right)+\hat{\mu}^N\left(\frac{\partial\boldsymbol{\Psi}^N}{\partial t}-\frac{\partial\boldsymbol{\Psi}^S}{\partial t}\right) \\ n_0^W\rho_0^W\frac{\partial^2\boldsymbol{\Psi}^W}{\partial t^2} = -\hat{\mu}^W\left(\frac{\partial\boldsymbol{\Psi}^W}{\partial t}-\frac{\partial\boldsymbol{\Psi}^S}{\partial t}\right) \\ n_0^N\rho_0^N\frac{\partial^2\boldsymbol{\Psi}^N}{\partial t^2} = -\hat{\mu}^N\left(\frac{\partial\boldsymbol{\Psi}^N}{\partial t}-\frac{\partial\boldsymbol{\Psi}^S}{\partial t}\right) \end{cases} \tag{7}$$

Assuming that the incident wave is a harmonic with circular frequency ω, the expressions of scalar potentials and vector potentials can be expressed as:

$$\varphi^\alpha = \varphi^\alpha(x,y,z)e^{-i\omega t}\Big) \tag{8a}$$

$$\boldsymbol{\Psi}^\alpha = \Psi^\alpha(x,y,z)e^{-i\omega t} \tag{8b}$$

By applying Equations (8a) and (8b), Equations (6) and (7) can be transformed into:

$$\begin{cases} (M_{SS}^*\nabla^2+\gamma_{SS}\omega^2)\varphi^S + (M_{SW}\nabla^2-\gamma_{SW}\omega^2)\varphi^W + (M_{SN}\nabla^2-\gamma_{SN}\omega^2)\varphi^N = 0 \\ (M_{SW}\nabla^2-\gamma_{SW}\omega^2)\varphi^S + (M_{WW}\nabla^2+\gamma_{WW}\omega^2)\varphi^W + M_{WN}\nabla^2\varphi^N = 0 \\ (M_{SN}\nabla^2-\gamma_{SN}\omega^2)\varphi^S + M_{WN}\nabla^2\varphi^W + (M_{NN}\nabla^2+\gamma_{NN}\omega^2)\varphi^N = 0 \end{cases} \tag{9}$$

$$\begin{cases} -\omega^2 n_0^S\rho_0^S\Psi^S = n_0^S\mu_S\nabla^2\Psi^S - i\omega\hat{\mu}^W\left(\Psi^W-\Psi^S\right) - i\omega\hat{\mu}^N\left(\Psi^N-\Psi^S\right) \\ -\omega^2 n_0^W\rho_0^W\Psi^W = i\omega\hat{\mu}^W\left(\Psi^W-\Psi^S\right) \\ -\omega^2 n_0^N\rho_0^N\Psi^N = i\omega\hat{\mu}^N\left(\Psi^N-\Psi^S\right) \end{cases} \tag{10}$$

where, $M_{SS}^* = M_{SS}+2n_0^S\mu_S$; $\gamma_{SS} = n_0^S\rho_0^S + \frac{i\,(\hat{\mu}^W+\hat{\mu}^N)}{\omega}$; $\gamma_{SW} = \frac{i\,\hat{\mu}^W}{\omega}$; $\gamma_{SN} = \frac{i\hat{\mu}^N}{\omega}$; $\gamma_{WW} = n_0^W\rho_0^W + \frac{i\hat{\mu}^W}{\omega}$; $\gamma_{NN} = n_0^N\rho_0^N + \frac{i\hat{\mu}^N}{\omega}$.

Eliminating φ^W and φ^N from Equation (9), the scalar potential of the solid component φ^S can be expressed as:

$$\left(A\nabla^6 + B\omega^2\nabla^4 + C\omega^4\nabla^2 + D\omega^6\right)\varphi^S = 0 \tag{11}$$

where,

$$\left.\begin{array}{l} A = M_{SS}^*A_3 + M_{SW}A_1 + M_{SN}A_2 \\ B = M_{SS}^*B_3 + M_{SW}B_1 + M_{SN}B_2 + \gamma_{SS}A_3 - \gamma_{SW}A_1 - \gamma_{SN}A_2 \\ C = M_{SS}^*C_3 + M_{SW}C_1 + M_{SN}C_2 + \gamma_{SS}B_3 - \gamma_{SW}B_1 - \gamma_{SN}B_2 \\ D = \gamma_{SS}C_3 - \gamma_{SW}C_1 - \gamma_{SN}C_2 \end{array}\right\} \tag{12}$$

with

$A_1 = M_{WN}M_{SN} - M_{SW}M_{NN}$, $B_1 = M_{NN}\gamma_{SW} - M_{SW}\gamma_{NN} - M_{WN}\gamma_{SN}$, $C_1 = \gamma_{NN}\gamma_{SW}$;
$A_2 = M_{SW}M_{WN} - M_{SN}M_{WW}$, $B_2 = M_{WW}\gamma_{SN} - M_{SN}\gamma_{WW} - M_{WN}\gamma_{SW}$, $C_2 = \gamma_{WW}\gamma_{SN}$;
$A_3 = M_{WW}M_{NN} - M_{WN}M_{WN}$, $B_3 = M_{WW}\gamma_{NN} + M_{NN}\gamma_{WW}$, $C_3 = \gamma_{WW}\gamma_{NN}$.

To solve the general solution of φ^S, Equation (11) can be decomposed into:

$$\left(\nabla^2 - k_j^2\right)\varphi_j^S = 0 (j = 1,2,3) \tag{13}$$

with

$$\begin{cases} k_1^2 = -\frac{\omega^2}{3A}\left(B - \frac{\left(1+\sqrt{3}i\right)A^*}{2C^*} + \frac{\left(1-\sqrt{3}i\right)}{2}C^*\right) \\ k_2^2 = -\frac{\omega^2}{3A}\left(B - \frac{\left(1-\sqrt{3}i\right)A^*}{2C^*} + \frac{\left(1+\sqrt{3}i\right)}{2}C^*\right) \\ k_3^2 = -\frac{\omega^2}{3A}\left(B + \frac{A^*}{C^*} - C^*\right) \end{cases} \tag{14}$$

where, $A^* = 3AC - B^2$; $B^* = 9ABC - 2B^3 - 27A^2D$; $C^* = \left[\frac{B^*}{2} + \sqrt[2]{(A^*)^3 + \left(\frac{B^*}{2}\right)^2}\right]^{1/3}$.

It can be seen from Equation (13) that there are three kinds of compression waves named P_1, P_2, and P_3 waves in unsaturated porous media. $k_i (i = 1, 2, 3)$ are the wave numbers associated with the three types of waves.

In cylindrical coordinates, Equation (13) can be expressed as:

$$\frac{\partial^2 \varphi_j^S}{\partial r^2} + \frac{1}{r}\frac{\partial \varphi_j^S}{\partial r} + \frac{1}{r^2}\frac{\partial^2 \varphi_j^S}{\partial \theta^2} - k_j^2 \varphi_j^S = 0 \tag{15}$$

By using the method of separating variables and according to Sommerfeld radiation condition [20], the solution $\varphi_j^S(r, \theta)$ is obtained as:

$$\varphi_j^S(r, \theta) = \sum_{n=0}^{\infty} A_{n,j} K_n(k_j r) \cos n\theta (j = 1, 2, 3) \tag{16}$$

where $K_n(k_j r)$ denotes the n-order modified Bessel functions of the first kind, $A_{n,j} (j = 1, 2, 3)$ is the undetermined constant coefficient.

Thus, it can be deduced that the scalar potential function of solid skeleton in unsaturated media is:

$$\varphi^S = \varphi_1^S + \varphi_2^S + \varphi_3^S \tag{17}$$

According to Equation (9), the transformation relation between the scalar potential functions of liquid and gas phase and the scalar potential function of solid skeleton are:

$$\varphi_j^W = \delta_j^W \varphi_j^S \tag{18}$$

$$\varphi_j^N = \delta_j^N \varphi_j^S \tag{19}$$

where

$$\delta_j^W = \frac{A_1 k_j^4 + B_1 \omega^2 k_j^2 + C_1 \omega^4}{A_3 k_j^4 + B_3 \omega^2 k_j^2 + C_3 \omega^4} (j = 1, 2, 3) \tag{20a}$$

$$\delta_j^N = \frac{A_2 k_j^4 + B_2 \omega^2 k_j^2 + C_2 \omega^4}{A_3 k_j^4 + B_3 \omega^2 k_j^2 + C_3 \omega^4} (j = 1, 2, 3) \tag{20b}$$

Thus, the scalar potential functions of fluid and gas can be determined as:

$$\varphi^W = \varphi_1^W + \varphi_2^W + \varphi_3^W = \delta_1^W \varphi_1^S + \delta_2^W \varphi_2^S + \delta_3^W \varphi_3^S \tag{21}$$

$$\varphi^N = \varphi_1^N + \varphi_2^N + \varphi_3^N = \delta_1^N \varphi_1^S + \delta_2^N \varphi_2^S + \delta_3^N \varphi_3^S \tag{22}$$

Doing the same thing for Equation (10), the solution of the vector potential of the solid component $\boldsymbol{\Psi}^S(r, \theta)$ in cylindrical coordinates can be obtained as:

$$\Psi^S(r, \theta) = \sum_{n=0}^{\infty} B_n K_n(k_4 r) \sin n\theta \tag{23}$$

where B_n is the undetermined constant coefficient, and k_4 is the wave number of the shear wave with:

$$k_4^2 = \frac{F\omega^2}{E} \tag{24}$$

where $E = n_0^S \mu_S \gamma_{WW} \gamma_{NN}$, $F = -\gamma_{SS}\gamma_{WW}\gamma_{NN} + \gamma_{SW}\gamma_{SW}\gamma_{NN} + \gamma_{SN}\gamma_{SN}\gamma_{WW}$.

The vector potentials of the liquid and gas phases can be expressed as:

$$\Psi^W = \zeta^W \Psi^S \tag{25}$$

$$\Psi^N = \zeta^N \Psi^S \tag{26}$$

where $\zeta^W = \frac{\gamma_{SW}}{\gamma_{WW}}$, $\zeta^N = \frac{\gamma_{SN}}{\gamma_{NN}}$.

2.3. Wave Field Analysis and Solutions

Assuming a plane harmonic P_1 or SV wave with circular frequency ω propagates in the positive direction of the x-axis, which may be expressed in terms of the Bessel-Fourier series:

$$\varphi^i = \varphi_0 \sum_{n=0}^{\infty} \varepsilon_n i^n J_n(k_0 r) \cos n\theta e^{-i\omega t} \tag{27}$$

$$\Psi^i = \Psi_0 \sum_{n=0}^{\infty} \varepsilon_n i^n J_n(k_0 r) \cos n\theta e^{-i\omega t} \tag{28}$$

where $k_0 = \omega / c_p$ (for P_1 wave incidence) or $k_0 = \omega / c_s$ (for SV wave incidence) represents the wave number of the incident wave, $\varphi_0(\Psi_0)$ represents the incident wave amplitude, $J_n(.)$ is the Bessel function of the first kind of order n, $\varepsilon_n = 1$ if $n = 0$ and $\varepsilon_n = 2$ if $n \geq 1$, and $i = \sqrt{-1}$.

When the incident plane wave is on the cavity surface, waveform conversion will occur, and the cavity surface will produce scattered waves. The total wave field in an unsaturated porous medium consists of incident waves and scattered waves. The potential of the total wave field in an unsaturated porous medium can be expressed as follows [18].

For the P_1 wave incidence, the total scalar potentials of each phase can be written as:

$$\begin{cases} \varphi^{\mathrm{S}}(r,\theta) = \sum\limits_{j=1}^{3} \sum\limits_{n=0}^{\infty} A_{n,j} K_n(k_j r) \cos n\theta + \varphi_0 \sum\limits_{n=0}^{\infty} \varepsilon_n i^n J_n(k_0 r) \cos n\theta \\ \varphi^{\mathrm{W}} = \sum\limits_{j=1}^{3} \delta_j^{\mathrm{W}} \sum\limits_{n=0}^{\infty} A_{n,j} K_n(k_j r) \cos n\theta + \delta_1^{\mathrm{W}} \varphi_0 \sum\limits_{n=0}^{\infty} \varepsilon_n i^n J_n(k_0 r) \cos n\theta \\ \varphi^{\mathrm{N}} = \sum\limits_{j=1}^{3} \delta_j^{\mathrm{N}} \sum\limits_{n=0}^{\infty} A_{n,j} K_n(k_j r) \cos n\theta + \delta_1^{\mathrm{N}} \varphi_0 \sum\limits_{n=0}^{\infty} \varepsilon_n i^n J_n(k_0 r) \cos n\theta \end{cases} \tag{29a}$$

The total vector potential functions can be written as:

$$\begin{cases} \Psi^{\mathrm{S}} = \sum\limits_{n=0}^{\infty} B_n K_n(k_4 r) \sin n\theta \\ \Psi^W = \zeta^W \Psi^S \\ \Psi^W = \zeta^W \Psi^S \end{cases} \tag{29b}$$

For the SV wave incidence, the total scalar potentials of each phase can be written as:

$$\begin{cases} \varphi^{\mathrm{S}}(r,\theta) = \sum\limits_{j=1}^{3} \sum\limits_{n=0}^{\infty} A_{n,j} K_n(k_j r) \cos n\theta \\ \varphi^{\mathrm{W}} = \sum\limits_{j=1}^{3} \delta_j^{\mathrm{W}} \sum\limits_{n=0}^{\infty} A_{n,j} K_n(k_j r) \cos n\theta \\ \varphi^{\mathrm{N}} = \sum\limits_{j=1}^{3} \delta_j^{\mathrm{N}} \sum\limits_{n=0}^{\infty} A_{n,j} K_n(k_j r) \cos n\theta \end{cases} \tag{30a}$$

The total vector potential functions can be written as:

$$\begin{cases} \Psi^{\mathrm{S}} = \sum\limits_{n=0}^{\infty} B_n K_n(k_4 r)\sin n\theta + \Psi_0 \sum\limits_{n=0}^{\infty} \varepsilon_n i^n J_n(k_0 r)\cos n\theta \\ \Psi^{\mathrm{W}} = \zeta^{\mathrm{W}} \Psi^{\mathrm{S}} \\ \Psi^{\mathrm{W}} = \zeta^{\mathrm{W}} \Psi^{\mathrm{S}} \end{cases} \tag{30b}$$

where $A_{n,j}(j = 1, 2, 3)$ and B_n refer to the unknown amplitudes of a P wave and an S wave, which should be determined by the boundary conditions.

Assuming the permeable boundary conditions of the cavity and the continuity conditions of the displacement between the fluid and the solid skeleton, the boundary conditions at the surface of the cavity ($r = a$) can be expressed as:

$$\sigma_{rr}^{\mathrm{S}} = \sigma_{rr}^{\mathrm{W}} = \sigma_{rr}^{\mathrm{N}} = \sigma_{r\theta}^{\mathrm{S}} = 0 (\text{at } r = a) \tag{31}$$

Substituting Equation (5) into the constitutive relations of Equation (4) in cylindrical coordinates [1], the stress and displacement components in Equation (31) can be expressed by the potentials of the total wave field. Substituting the expressions of the potentials of the total wave field, Equation (29), or Equation (30) into the boundary conditions with the stress components being expressed by the potentials of the total wave field, a system of linear equations about unknown quantity, $A_{n,j}$ $(j = 1, 2, 3)$ and B_n , can be obtained as follows,

For P_1 wave incidence:

$$\left[\begin{array}{cccc} S_1 & S_2 & S_3 & S_5 \\ W_1 & W_2 & W_3 & W_5 \\ X_1 & X_2 & X_3 & X_5 \\ Y_1 & Y_2 & Y_3 & Y_5 \end{array} \right]\Bigg|_{r=a} \left[\begin{array}{c} A_{n,1} \\ A_{n,2} \\ A_{n,3} \\ B_n \end{array} \right] = \left[\begin{array}{c} -S_4 \\ -W_4 \\ -X_4 \\ -Y_4 \end{array} \right]\Bigg|_{r=a} \tag{32}$$

For SV wave incidence:

$$\left[\begin{array}{cccc} S_1 & S_2 & S_3 & S_4 \\ W_1 & W_2 & W_3 & W_4 \\ X_1 & X_2 & X_3 & X_4 \\ Y_1 & Y_2 & Y_3 & Y_4 \end{array} \right]\Bigg|_{r=a} \left[\begin{array}{c} A_{n,1} \\ A_{n,2} \\ A_{n,3} \\ B_n \end{array} \right] = \left[\begin{array}{c} -S_5 \\ -W_5 \\ -X_5 \\ -Y_5 \end{array} \right]\Bigg|_{r=a} \tag{33}$$

The detailed expressions of coefficients S_j, W_j, X_j, and Y_j as provided in Appendix A. By solving Equations (32) and (33) for different kinds of incident waves, respectively, the undetermined wave amplitude coefficients $A_{n,j}$ $(j = 1, 2, 3)$ and B_n can be obtained by solving the system of linear equations. Once the undetermined wave amplitude coefficients are obtained, the scattered wave field can be calculated. Finally, the displacement and stress components can be obtained by the superposition of the incident wave and the scattered wave field.

3. Numerical Results and Discussion

From the perspective of engineering seismic resistance, the main goal of the research is to study the dynamic response at the surface of the cavity, which is focused on the dynamic stress concentration factor.

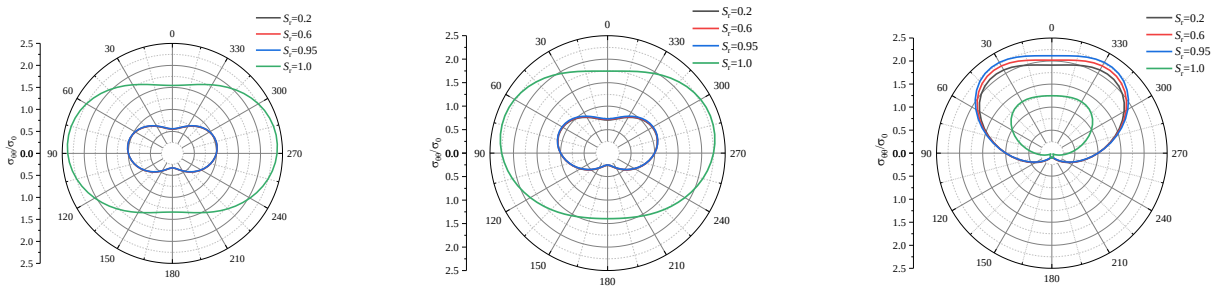
Take P_1 wave incidence for example, the influence of the saturation on the hoop stress concentration factor ($\sigma_{\theta\theta}^{S}/\sigma_0$) of the unsaturated porous medium at the cavity surface will be studied under both the impermeable and permeable conditions next. σ_0 is the maximum amplitude of hoop stress of the solid phase, owing to the incident wave at the same position. The material parameters are set per Lin (2005) [21] and listed in Table 1. A dimensionless frequency $k_0 a$ determined by the wavelength and the cavity radius is introduced.

Table 1. Material parameters of the unsaturated porous medium.

Porosity n_0	**0.1**	**0.34**	**0.36**
ρ_0^{S} (kg/m^3)	2650	2650	2650
ρ_0^{W} (kg/m^3)	1000	1000	1000
ρ_0^{N} (kg/m^3)	1.1	1.1	1.1
K_{S} (kPa)	3.6×10^7	3.6×10^7	3.6×10^7
K_{W} (kPa)	2.0×10^6	2.0×10^6	2.0×10^6
K_{N} (kPa)	110	110	110
ν^{W} (Pa·s)	1.0×10^{-3}	1.0×10^{-3}	1.0×10^{-3}
ν^{N} (Pa·s)	1.8×10^{-5}	1.8×10^{-5}	1.8×10^{-5}
κ (m·s^{-1})	2.5×10^{-12}	2.5×10^{-12}	2.5×10^{-12}
G	1.203×10^7	–	9.23×10^4
α_{B}	1	1	1
$\hat{K}$ (kPa)	2.6055×10^7	2.189×10^6	2.0×10^5
υ	0.3	0.1, 0.2, 0.3	0.3
α	2.0×10^{-5}	2.0×10^{-5}	2.0×10^{-5}
d	4.15	4.15	4.15
S_{rW}	0.05	0.05	0.05
S_{rN}	1.0	1.0	1.0

(1) The influence of saturation S_{r} on the dynamic response of the cavity

Taking the second set of parameters in Table 1 with Poisson's ratio $\upsilon = 0.3$ and the different saturations $S_{\mathrm{r}} = 0.2, 0.6, 0.95, 1.0$ under different frequencies $k_0 a = 0.5, 1.0, 3.0$, Figures 2 and 3 show the distributions of $\sigma_{\theta\theta}^{\mathrm{S}}/\sigma_0$ around the surface of the cavity for the P_1 wave incidence under impermeable and permeable conditions, respectively. Considering that the P_1 wave velocity of the unsaturated porous medium varies greatly with the saturation, here, k_0 is taken as the wave number of the S wave for $S_{\mathrm{r}} = 1.0$.

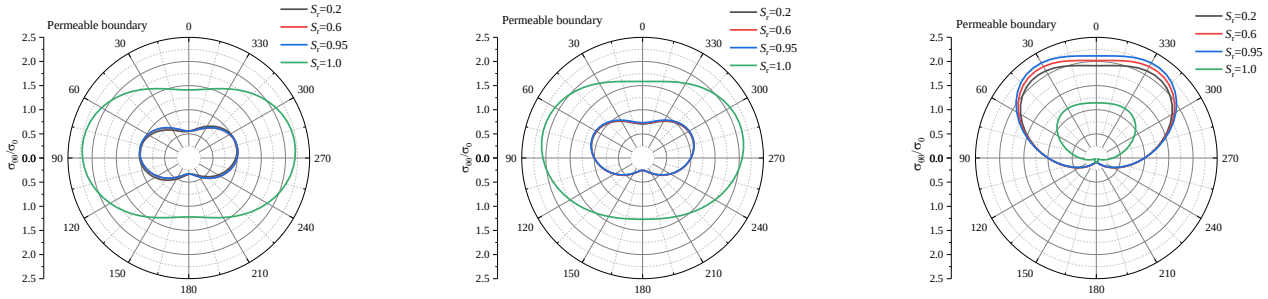


(**a**) (**b**) (**c**)

Figure 2. Effects of saturation on distributions of $\sigma_{\theta\theta}^{\mathrm{S}}/\sigma_0$ around the surface of the cavity for P_1 wave incidence with the second set of parameters in Table 1 with $\upsilon = 0.3$ for an impermeable boundary. (**a**) $k_0 a = 0.5$. (**b**) $k_0 a = 1.0$. (**c**) $k_0 a = 3.0$.

As shown in the figure, for both the impermeable and permeable conditions, the stress distribution around the cavity is symmetrical on both sides of the incident wave. The response of the stress around the cavity for $S_{\mathrm{r}} = 1.0$ is significantly different from that for $S_{\mathrm{r}} = 1.0$. When $S_{\mathrm{r}} < 0$, the saturation has little effect on the distribution of stress around the cavity, especially at low-frequency incidence. It means that the existence of the gas phase significantly affects the dynamic response of the cavity in the unsaturated medium. The main reason for the effect is that the existence of the gas phase will significantly affect the wave velocity of the P wave in the unsaturated medium [14]. The stress distribution around the cavity changes significantly with the change of the frequency of the incident wave. At low-frequency incidence ($k_0 a = 0.2$), the maximum appears slightly deviated from the orthogonal direction ($\theta = 80^\circ$ and 280°). With the increase in the incident frequency, the direction in which the maximum value occurs gradually approaches the direction of

the incident wave ($\theta = 0°$). At high-frequency incidence ($k_0a = 3.0$), for $S_r < 1.0$, the stress peaks at $\theta = 35°$ and 325°, and for $S_r = 1.0$, the stress peaks at $\theta = 30°$ and 330°. The minimum stress appears in the opposite direction of the incident wave ($\theta = 180°$) for $S_r < 1.0$ under all incident frequencies and S_r =1.0 under $k_0a = 0.5$, 1.0. Under $k_0a = 3.0$, The minimum stress for $S_r = 1.0$ occurs at $\theta = 130°$ and 230°. With the increase in the incident frequency, the effects of the saturation on the dynamic stress concentration factor increase. Under $k_0a = 0.5$, 1.0, the dynamic stress concentration factors for $S_r = 1.0$ are larger than that for $S_r < 1.0$. However, under $k_0a = 3.0$, the result is the opposite. When $S_r < 1.0$, the dynamic stress concentration factor increases slightly with the increase in the saturation degree.



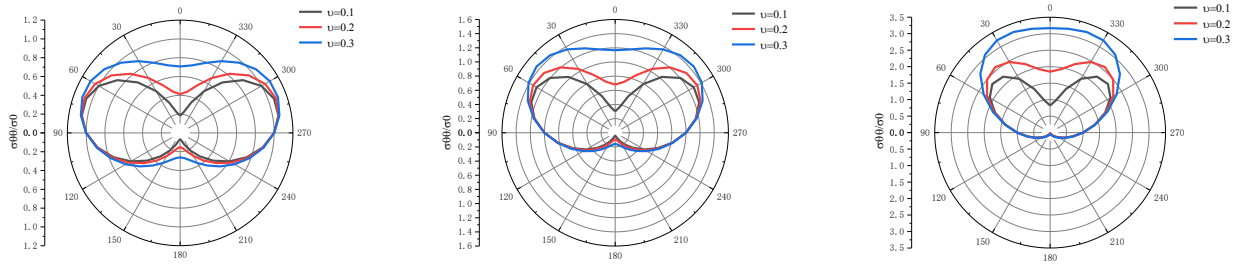
(**a**) (**b**) (**c**)

Figure 3. Effects of saturation on distributions of $\sigma^S_{\theta\theta}/\sigma_0$ around the surface of the cavity for P_1 wave incidence with the second set of parameters in Table 1 with υ = 0.3 s for a permeable boundary. (**a**) k_0a = 0.5. (**b**) k_0a = 1.0. (**c**) k_0a = 3.0.

By comparing the permeable and impermeable boundary conditions, the dynamic stress concentration factor of an impermeable cavity is slightly larger than that of a permeable cavity for S_r = 1.0. For $S_r < 1.0$, there are no obvious differences between the dynamic stress concentration factors of the permeable and impermeable cavities.

(2) The influence of Poisson's ratio on the dynamic responses of the cavity

Taking the second set of parameters in Table 1 with S_r = 0.6, Figure 4 gives the distributions of $\sigma^S_{\theta\theta}/\sigma_0$ around the cavity surface for P_1 wave incidence for different Poisson's ratios of υ = 0.1, 0.2, and 0.3 with k_0a = 0.5, 1.0, and 2.0 under impermeable conditions, respectively. As can be seen from the figure, with the increase in Poisson's ratio, the stress increases gradually under different frequencies, and the angle at which the maximum value occurs gradually approaches the direction of the incident wave direction. For example, when k_0a = 2.0, the maximum values for υ = 0.1 occur at $\theta = 50°$ and 310°, whereas for υ = 0.2, at $\theta = 40°$ and 320°, and for υ = 0.3, at $\theta = 20°$ and 340°. For all Poisson's ratios, the minimum values appear at $\theta = 180°$. Moreover, with the increase in the incident frequency, the angle between the maximum value direction and the incident wave direction ($\theta = 0°$) decreases at the same Poisson's ratio. For υ = 0.3, the maximum values appear at $\theta = 70°$ and 290° when k_0a = 0.5, at $\theta = 40°$ and 320° when k_0a = 1.0, and at $\theta = 20°$ and 340° when k_0a = 2.0.

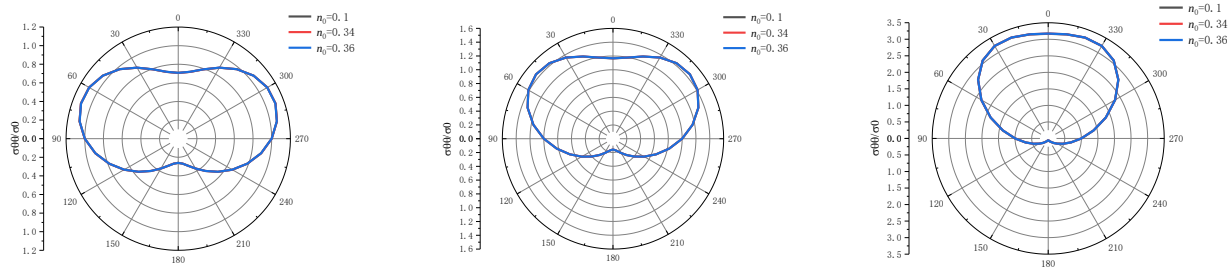


(**a**) (**b**) (**c**)

Figure 4. Effects of Poisson's ratio on distributions of $\sigma^S_{\theta\theta}/\sigma_0$ around the surface of the cavity for P_1 wave incidence with the second set of parameters in Table 1 with $S_r = 0.6$. (**a**) $k_0a = 0.5$. (**b**) $k_0a = 1.0$. (**c**) $k_0a = 2.0$.

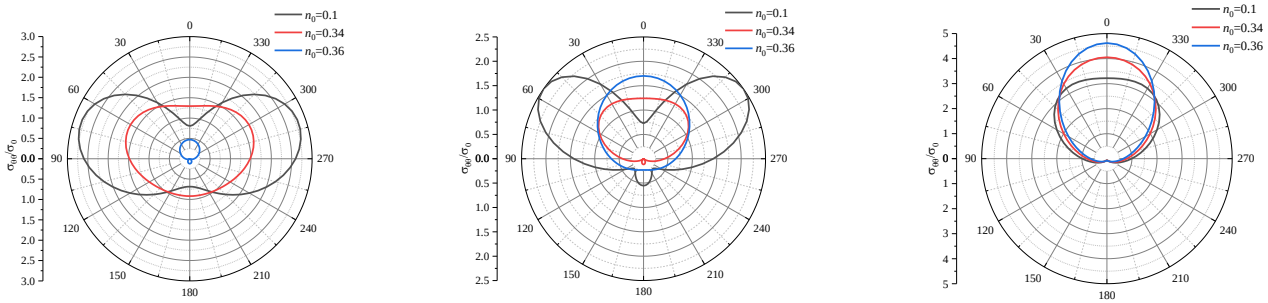
(3) The influence of porosity on the dynamic responses of the cavity

According to Ref. [21], the volume modulus $\hat{K}$ and shear modulus G of solid skeletons decrease with the increase in porosity n_0, which will make the wave number change, and thus, the stress around the cavity will change accordingly. Next, the effects of porosity n_0 on the dynamic responses around the cavity under two saturation conditions, $S_r = 0.6$ and 1.0, are analyzed for the impermeable cavity. Taking the three sets of parameters in Table 1 with $v = 0.3$, Figure 5 gives the distributions of $\sigma^S_{\theta\theta}/\sigma_0$ around the cavity surface for the P_1 wave incidence under $n_0 = 0.1$, 0.34, and 0.36 for $S_r = 0.6$ with $k_0a = 0.5$, 1.0, and 2.0, respectively. As can be seen from the figure, when $S_r = 0.6$, the porosity n_0 does not affect the distribution of $\sigma^S_{\theta\theta}/\sigma_0$. That means, for $S_r = 0.6$, although porosity will affect the stiffness of the medium, thus affecting the dynamic stress, it will not affect the dynamic stress concentration factor. This is because Poisson's ratio does not change with porosity in the analysis. According to Ref. [14], the velocity of the P1 wave has a sharp decline from a fully saturated condition ($S_r = 1.0$) to an unsaturated condition ($S_r < 1.0$). However, the velocity of the S wave changes little with the saturation. For $S_r < 1.0$, the ratio of the P_1 wave velocity to the S wave velocity is only related to Poisson's ratio, but not to porosity. When the frequency is normalized as k_0a, the effect of the stiffness on the wave number is eliminated. As Poisson's ratio does not change with the porosity, the change in the stiffness of the surrounding medium with the porosity certainly will not influence the normalized hoop stresses. Figure 6 gives the distributions of $\sigma^S_{\theta\theta}/\sigma_0$ around the cavity surface for the P_1 wave incidence under $n_0 = 0.1$, 0.34, and 0.36 for $S_r = 1.0$ with $k_0a = 0.5$, 1.0, and 2.0, respectively. Here, k_0 is taken as the wave number of the incident P_1 wave. It can be seen that when $S_r = 1.0$, the porosity has a great influence on the dynamic stress concentration factor. The distribution pattern of $\sigma^S_{\theta\theta}/\sigma_0$ around the cavity surface varies greatly for different porosities. This situation is different from that of unsaturated ($S_r < 1.0$). That is mainly because that the ratio of P_1 wave velocity to S wave velocity varies greatly with the porosity of the saturated poroelastic medium. According to Ref. [21], when $n_0 = 0.1$, the ratio of the P_1 wave velocity to the S wave velocity is nearly $\sqrt{\frac{2(1-v)}{1-2v}} = 1.87$. With the increase in the porosity, the ratio of the P_1 wave velocity to the S wave velocity increases a lot. For example, the ratio can reach 7.58 for $n_0 = 0.36$. To find the rules of the effects of porosity on the distribution of the dynamic stress concentration factor, by taking k_0 as the wave number of the SV wave, Figure 7 gives the distributions of $\sigma^S_{\theta\theta}/\sigma_0$ around the cavity surface for P_1 wave incidence under $n_0 = 0.1$, 0.34, and 0.36 for $S_r = 1.0$ with $k_0a = 0.5$, 1.0, and 3.0, respectively. As seen in the figure, with the increase in the porosity, the distribution of the dynamic stress concentration factor tends to be uniform along the circumference. When the porosity is large, the maximum value of the dynamic stress concentration factor is relatively small.



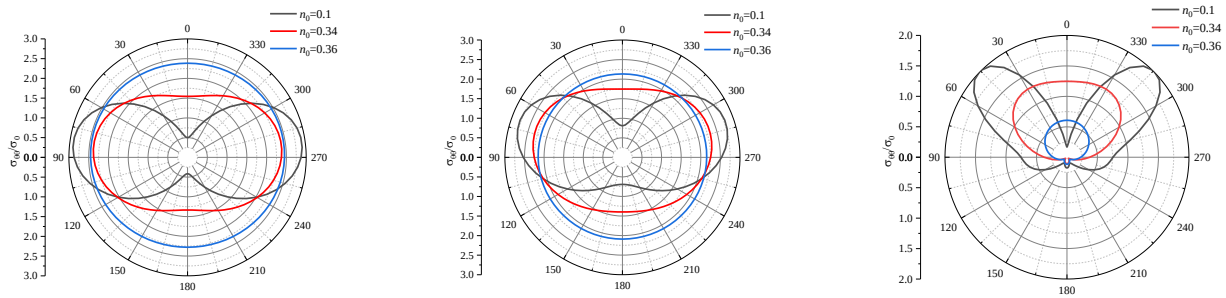
(**a**) (**b**) (**c**)

Figure 5. Effects of porosities on distributions of $\sigma^S_{\theta\theta}/\sigma_0$ around the surface of the cavity for P_1 wave incidence for S_r = 0.6. (**a**) k_0a= 0.5. (**b**) k_0a= 1.0. (**c**) k_0a= 2.0.



(**a**) (**b**) (**c**)

Figure 6. Effects of porosities on distributions of $\sigma^S_{\theta\theta}/\sigma_0$ around the surface of the cavity for P_1 wave incidence for S_r = 1.0. (k_0 is the wave number of the incident P1 wave). (**a**) k_0a= 0.5. (**b**) k_0a= 1.0. (**c**) k_0a= 2.0.



(**a**) (**b**) (**c**)

Figure 7. Effects of porosities on distributions of $\sigma^S_{\theta\theta}/\sigma_0$ around the surface of the cavity for P_1 wave incidence for S_r = 1.0. (k_0 is the wave number of the SV wave). (**a**) k_0a = 0.5. (**b**) k_0a = 1.0. (**c**) k_0a = 3.0.

4. Conclusions

In this research, the scattering of plane waves (P and SV waves) by a cylindrical cavity with a permeable surface in an unsaturated poroelastic medium was solved based on Ref. [17]. The results can be used to calculate the dynamic stress concentration factor around the cavity. The influences of saturation, porosity, and Poisson's ratio on the dynamic stress concentration factor around the cavity under different incident frequencies and boundary conditions were studied in detail. The main conclusions are as follows,

The distributions of the hoop stress around the surface of the cavity change with saturation. The responses of the stress around the cavity for S_r = 1.0 are significantly different from that for S_r < 1.0. When S_r < 1.0, saturation has little effect on the distribution

of stress. For the same saturation, the frequency of the incident wave will change the angle at which the maximum value occurs.

For S_r = 1.0, the dynamic stress concentration factor of an impermeable cavity is slightly larger than that of a permeable cavity. For S_r < 1.0, the responses have no obvious differences between the permeable and impermeable cavities.

The distribution of stress around the cavity varies with Poisson's ratio. With the increase in Poisson's ratio, the dynamic stress concentration factor around the cavity increases gradually, and the angle at which the maximum value occurs gradually approaches the direction of the incident wave direction.

The porosity does not affect the dynamic stress concentration factor around the cavity for an unsaturated medium. However, it has great influences on the hoop stress distribution around the cavity for S_r = 1.0. That is mainly because the ratio of the P_1 wave velocity to the S wave velocity varies greatly with the porosity of the saturated poroelastic medium.

Author Contributions: Conceptualization, W.L.; methodology, W.L. and F.F.; software, Z.Y. and F.F.; validation, F.F.; formal analysis, W.L.; investigation, W.L.; resources, W.L.; data curation, W.L. and Z.Y.; writing—original draft preparation, Z.Y. and A.Z.; writing—review and editing, W.L.; visualization, W.L. and Z.Y.; supervision, W.L.; project administration, W.L.; funding acquisition, W.L. All authors have read and agreed to the published version of the manuscript.

Funding: This work was supported by the Fundamental Research Funds for the Central Universities (Grant No. 2022JBZY010) and the National Natural Science Foundation of China (Grant No. 52078033).

Institutional Review Board Statement: Not applicable.

Informed Consent Statement: Not applicable.

Data Availability Statement: The data used in this study are available from the corresponding author upon reasonable request.

Conflicts of Interest: The authors declare no conflict of interest.

Appendix A

The expressions of coefficients S_j, W_j, X_j, and Y_j in Equations (32) and (33) are as follows: $S_1 = M_{SS}L_n^{21} + M_{SW}\delta_1^W L_n^{21} + M_{SN}\delta_1^N L_n^{21} + 2n_0^S\mu_S N_n^{21}$ (For P_1 wave incidence),

$S_2 = M_{SS}L_n^{22} + M_{SW}\delta_2^W L_n^{22} + M_{SN}\delta_2^N L_n^{22} + 2n_0^S\mu_S N_n^{22}$ (For SV wave incidence),

$S_3 = M_{SS}L_n^{23} + M_{SW}\delta_3^W L_n^{23} + M_{SN}\delta_3^N L_n^{23} + 2n_0^S\mu_S N_n^{23}$,

$S_4 = \varphi_0\varepsilon_n i^n\left(M_{SS}L_n^{10} + M_{SW}\delta_1^W L_n^{10} + M_{SN}\delta_1^N L_n^{10} + 2n_0^S\mu_S N_n^{10}\right)$ (For P_1 wave incidence),

$S_4 = \frac{2n_0^S\mu_S}{r^2}nE_n^{24} - \frac{2n_0^S\mu_S}{r}nM_n^{24}$ (For SV wave incidence),

$S_5 = \frac{2n_0^S\mu_S}{r}nM_n^{24} - \frac{2n_0^S\mu_S}{r^2}nE_n^{24}$ (For P_1 wave incidence),

$S_5 = \Psi_0\varepsilon_n i^n n\left(\frac{2n_0^S\mu_S}{r^2}E_n^{10} - \frac{2n_0^S\mu_S}{r}M_n^{10}\right)$ (For SV wave incidence).

$W_1 = M_{SW}L_n^{21} + M_{WW}\delta_1^W L_n^{21} + M_{WN}\delta_1^N L_n^{21}, W_2 = M_{SW}L_n^{22} + M_{WW}\delta_2^W L_n^{22} + M_{WN}\delta_2^N L_n^{22}$,

$W_3 = M_{SW}L_n^{23} + M_{WW}\delta_3^W L_n^{23} + M_{WN}\delta_3^N L_n^{23}, W_4 = \varphi_0\varepsilon_n i^n\left(M_{SW}L_n^{10} + M_{WW}\delta_1^W L_n^{10} + M_{WN}\delta_1^N L_n^{10}\right)$.

$X_1 = M_{SN}L_n^{21} + M_{WN}\delta_1^W L_n^{21} + M_{NN}\delta_1^N L_n^{21}, X_2 = M_{SN}L_n^{22} + M_{WN}\delta_2^W L_n^{22} + M_{NN}\delta_2^N L_n^{22}$,

$X_3 = M_{SN}L_n^{23} + M_{WN}\delta_3^W L_n^{23} + M_{NN}\delta_3^N L_n^{23}, X_4 = \varphi_0\varepsilon_n i^n L_n^{10}\left(M_{SN} + M_{WN}\delta_1^W + M_{NN}\delta_1^N\right)$.

$W_5 = X_5 = 0$.

$Y_1 = \frac{2n_0^S\mu_S}{r^2}nE_n^{21} - \frac{2n_0^S\mu_S}{r}nM_n^{21}$ (For P_1 wave incidence),

$Y_1 = \frac{2n_0^S\mu_S}{r}nM_n^{21} - \frac{2n_0^S\mu_S}{r^2}nE_n^{21}$(For SV wave incidence),

$Y_2 = \frac{2n_0^S\mu_S}{r^2}nE_n^{22} - \frac{2n_0^S\mu_S}{r}nM_n^{22}$ (For P_1 wave incidence),

$Y_2 = \frac{2n_0^S\mu_S}{r}nM_n^{22} - \frac{2n_0^S\mu_S}{r^2}nE_n^{22}$ (For SV wave incidence),

$Y_3 = \frac{2n_0^S\mu_S}{r^2}nE_n^{23} - \frac{2n_0^S\mu_S}{r}nM_n^{23}$,

$Y_4 = \varphi_0\varepsilon_n i^n\left(\frac{2n_0^S\mu_S}{r^2}nE_n^{10} - \frac{2n_0^S\mu_S}{r}nM_n^{10}\right)$ (For P_1 wave incidence),

$Y_4 = -\frac{n_0^S\mu_S}{r^2}n^2E_n^{24} - n_0^S\mu_S N_n^{24} + \frac{n_0^S\mu_S}{r}M_n^{24}$ (For SV wave incidence),

$Y_5 = \frac{n_0^S\mu_S}{r}M_n^{24} - \frac{n_0^S\mu_S}{r^2}n^2E_n^{24} - n_0^S\mu_S N_n^{24}$ (For P_1 wave incidence),

$Y_5 = \mathbf{\Psi}_0 \varepsilon_n i^n \left(-\frac{n_0^S \mu_S}{r^2} n^2 E_n^{10} - n_0^S \mu_S N_n^{10} + \frac{n_0^S \mu_S}{r} M_n^{10} \right)$ (For SV wave incidence).

with $E_n^{10} = J_n(k_0 r)$, $E_n^{21} = K_n(k_1 r)$, $E_n^{23} = K_n(k_3 r)$, $E_n^{24} = K_n(k_4 r)$, $M_n^{ij} = \frac{dE_n^{ij}}{dr}$, $N_n^{ij} = \frac{d^2 E_n^{ij}}{dr^2}$, and L_n^{ij} represents the Laplacian ∇^2.

References

1. Pao, Y.H.; Mow, C.C. *Diffraction of Elastic Waves and Dynamic Stress Concentrations*; Crane Russa: New York, NY, USA, 1973.
2. Lee, V.W.; Trifunac, M.D. Response of taunnels to incident SH waves. *J. Eng. Mech. Div.* **1979**, *105*, 643–659. [CrossRef]
3. Lee, V.W.; Karl, J. Diffraction of SV waves by underground, circular, cylindrical cavities. *Soil Dyn. Earthq. Eng.* **1992**, *11*, 445–456. [CrossRef]
4. Lee, V.W.; Karl, J. On deformation near a circular underground cavity subjected to incident plane P waves. *Eur. J. Earthq. Eng.* **1993**, *11*, 29–36.
5. Biot, M.A. Theory of propagation of elastic wave in fluid-saturated porous soil (I. 1ower-frequency range). *J. Acoust. Soc. Am.* **1956**, *28*, 168–191. [CrossRef]
6. Mei, C.C.; Si, B.I.; Cai, D. Scattering of simple harmonic waves by a circular cavity in a fluid-infiltrated poro-elastic medium. *Wave Motion* **1984**, *6*, 265–278. [CrossRef]
7. Krutin, V.N.; Markov, M.G.; Yumatov, A.Y. Normal waves in a fluid-filled cylindrical cavity located in a saturated porous medium. *J. Appl. Math. Mech.* **1988**, *52*, 67–74. [CrossRef]
8. Shiba, Y.; Okamoto, S. Proposal of practical earthquake response analysis method of cylindrical tunnels in soft ground. *NIST* **1992**, *840*, 19–33.
9. Kattis, S.E.; Beskos, D.E.; Cheng, A.H.D. 2D dynamic response of unlined and lined tunnels in poroelastic soil to harmonic body waves. *Earthq. Eng. Struct. Dyn.* **2003**, *32*, 97–110. [CrossRef]
10. Li, W.H.; Zhao, C.G. An analytical solution for diffraction of plane P-waves by cylindrical cavity in a fluid-saturated porous media semi-space. *Rock Soil Mech.* **2004**, *25*, 1867–1872. (In Chinese)
11. Jiang, L.F.; Zhou, X.L.; Wang, J.H. Scattering of a plane wave by a lined cylindrical cavity in a poroelastic half-plane. *Comput. Geotech.* **2009**, *36*, 773–778. [CrossRef]
12. Xu, C.J.; Ding, H.B.; Tong, L.H.; Luo, W.J.; Wang, N. Scattering of a plane wave by shallow buried cylindrical lining in a poroelastic half-space. *Appl. Math. Model.* **2019**, *70*, 171–189. [CrossRef]
13. Schanz, M. Poroelasto dynamics: Linear models, analytical solutions, and numerical methods. *Appl. Mech. Rev.* **2009**, *62*, 030803. [CrossRef]
14. Li, W.H.; Zheng, J.; Trifunac, M.D. Saturation effects on ground motion of unsaturated soil layer—Bedrock system excited by plane P and SV waves. *Soil Dyn. Earthq. Eng.* **2018**, *37*, 482–492. [CrossRef]
15. Li, W.H.; Jia, X.; Feng, F.C.; Xu, Z. Axisymmetric transient response of a cylindrical cavity in an unsaturated poroelastic medium. *J. Sound Vib.* **2022**, *524*, 116763. [CrossRef]
16. Tan, Y.; Yang, M.S.; Li, X.Y. Dynamic response of a circular lined tunnel with an imperfect interface embedded in the unsaturated poroelastic medium under P wave. *Comput. Geotech.* **2020**, *122*, 103514. [CrossRef]
17. Zhang, A.C.; Li, W.H.; Feng, F.C. Scattering of incident plane waves by underground cylindrical cavity in unsaturated poroelastic medium. In Proceedings of the 4th International Conference on Performance-Based Design in Earthquake Geotechnical Engineering (PBD-IV), Beijing, China, 15–17 July 2022.
18. Wei, C.F.; Muraleetharan, K.K. A continuum theory of porous media saturated by multiple immiscible fluids. I. Linear poroelasticity. *Int. J. Eng. Sci.* **2002**, *40*, 1807–1833. [CrossRef]
19. van Genuchten, M.T. A closed-form equation for predicting the hydraulic conductivity of unsaturated soils. *Soil. Sci. Soc. Am. J.* **1980**, *44*, 892–898. [CrossRef]
20. Minskii, V. Sommerfeld radiation condition for second-order differential operator in a domain with infinite border. *J. Differ. Equ.* **1983**, *48*, 157–176. [CrossRef]
21. Lin, C.H.; Lee, V.W.; Trifunac, M.D. The reflection of plane waves in a poroelastic half space saturated with inviscid fluid. *Soil Dyn. Earthq. Eng.* **2005**, *25*, 205–223. [CrossRef]

Disclaimer/Publisher's Note: The statements, opinions and data contained in all publications are solely those of the individual author(s) and contributor(s) and not of MDPI and/or the editor(s). MDPI and/or the editor(s) disclaim responsibility for any injury to people or property resulting from any ideas, methods, instructions or products referred to in the content.